



HHS Public Access

Author manuscript

Science. Author manuscript; available in PMC 2016 July 08.

Published in final edited form as:

Science. 2016 January 8; 351(6269): aaa5694. doi:10.1126/science.aaa5694.

Gating of Hippocampal Activity, Plasticity and Memory by Entorhinal Cortex Long-Range Inhibition

Jayeeta Basu^{1,*#}, Jeffrey D. Zaremba^{1,^}, Stephanie K. Cheung^{1,#,^}, Frederick L. Hitti¹, Boris V. Zemelman², Attila Losonczi¹, and Steven A. Siegelbaum^{1,*}

¹Department of Neuroscience, Kavli Brain Institute, Columbia University Medical Center, 1051 Riverside Dr., New York, NY 10032, USA

²University of Texas, Austin, USA

Abstract

The cortico-hippocampal circuit is critical for storage of associational memories. Most studies have focused on the role in memory storage of the excitatory projections from entorhinal cortex to hippocampus. However, entorhinal cortex also sends inhibitory projections, whose role in memory storage and cortico-hippocampal activity remains largely unexplored. We found that these long-range inhibitory projections enhance the specificity of contextual and object memory encoding. At the circuit level, the GABAergic projections act as a disinhibitory gate that transiently promotes the excitation of hippocampal CA1 pyramidal neurons by suppressing feedforward inhibition. This enhances the ability of CA1 neurons to fire synaptically-evoked dendritic spikes and generate a temporally precise form of heterosynaptic plasticity. Long-range inhibition from entorhinal cortex may thus increase the precision of hippocampal-based longterm memory associations by assessing the salience of mnemonic information to the immediate sensory input.

One Sentence Summary

Long-range GABAergic input from lateral entorhinal cortex provides a precisely timed disinhibitory gate to trigger dendritic spikes, induce long-term heterosynaptic plasticity and specify contextual and object memory associations.

STRUCTURED ABSTRACT

Introduction—The precise association of contextual cues with a behavioral experience enables an animal to discriminate between salient (harmful or rewarding) versus neutral environments. What signaling mechanisms during learning help select specific contextual signals to be stored as long-term memories? Hippocampal CA1 pyramidal neurons integrate direct multisensory excitatory input from entorhinal cortex (EC) with indirect, mnemonic excitatory input from the upstream hippocampal CA3 area, and both pathways have been implicated in memory storage. Paired activation of the direct and indirect inputs at a precise timing interval that matches the dynamics of the cortico-hippocampal circuit induces a long-term enhancement of the

*Correspondence to: JB, jayeeta.basu@nyumc.org and SAS, sas8@columbia.edu.

#Present Address: Department of Neuroscience and Physiology, NYU Neuroscience Institute, New York University School of Medicine, 450 East 29th St, New York, NY 10016, USA

[^]Equal contribution

activation of CA1 neurons by their CA3 inputs (input-timing-dependent plasticity or ITDP). However, EC additionally sends long-range inhibitory projections (LRIPs) to CA1 whose function is largely unknown. Here we explore the role of the LRIPs in regulating hippocampal synaptic activity and memory.

Rationale—GABAergic neurons in medial entorhinal cortex (MEC) were recently found to send to hippocampus LRIPs that form relatively weak and sparse synapses on CA1 GABAergic interneurons. As lateral entorhinal cortex (LEC) conveys important contextual and object-related information to hippocampus, we examined whether this region also sends LRIPs to CA1. We expressed channelrhodopsin (ChR2) selectively in LEC inhibitory neurons and examined the synaptic effects of LRIP photostimulation.. The behavioral impact of the LRIPs was determined by selectively silencing these inputs locally in CA1 during contextual fear conditioning (CFC) and novel object recognition (NOR) tasks. We also used *in vivo* Ca^{2+} imaging to assess how different sensory and behavioral stimuli that typically comprise a contextual experience activate the LEC LRIPs. Finally, we examined how the LRIPs influence information flow through the cortico-hippocampal circuit and contribute to ITDP.

Results—LRIPs from LEC produced strong inhibitory postsynaptic potentials in a large fraction of CA1 interneurons located in the region of the EC inputs. Although pharmacogenetic silencing of LRIPs in hippocampus did not prevent CFC or NOR memory, it caused mice to show an inappropriate fear response to a neutral context and a diminished ability to distinguish a novel object from a familiar object. Calcium imaging revealed that the LRIP axons and presynaptic terminals responded to various sensory stimuli. Moreover, pairing such signals with appetitive or aversive stimuli increased LRIP activity, consistent with a role of the LRIPs in memory specificity.

Intracellular recordings demonstrated that the LRIPs powerfully suppressed the activity of a subclass of cholecystokinin-expressing interneurons (CCK+ INs). These interneurons were normally strongly excited by the CA3 inputs, resulting in pronounced feedforward inhibition (FFI) of CA1 pyramidal neuron dendrites. By transiently and maximally suppressing the INs in a 15–20 ms temporal window, the LRIPs enhanced CA3 inputs onto CA1 pyramidal neurons that arrived within that timing interval. This disinhibition enabled temporally precise, paired activation of EC-SC inputs (15–20 ms apart) to trigger dendritic spikes in the distal dendrites of CA1 PNs and induce ITDP.

Conclusions—LRIPs from EC act as a powerful, temporally precise disinhibitory gate of intra-hippocampal information flow and enable the induction of plasticity when cortical and hippocampal inputs arrive onto CA1 PNs at a precise 20 ms interval. We propose that the LRIPs increase the specificity of hippocampal-based long-term memory by assessing the salience of mnemonic information relayed by CA3 to the immediate sensory context conveyed by direct excitatory EC inputs.

The cortico-hippocampal circuit mediates the encoding and storage of specific associative memories, in part, through long-term plastic changes at neural circuit synapses. Most studies to date have focused on the importance of excitatory projections from entorhinal cortex (EC) to hippocampal CA1 pyramidal neurons, which provide the principal output of hippocampus(1–3). However, EC also sends long-range inhibitory projections (LRIPs) to the CA1 region of the hippocampus(4). At present, little is known about the role of these LRIPs in regulating hippocampal circuit operations, synaptic plasticity or memory storage.

Glutamatergic input to the CA1 region arrives from EC through both a direct and indirect pathway (5). In the indirect, or trisynaptic, path EC LII stellate cells excite dentate gyrus granule cells, which excite CA3 pyramidal neurons. The Schaffer collateral (SC) axons of CA3 pyramidal neurons provide strong excitatory drive onto CA1 pyramidal neurons by forming synapses on CA1 apical dendrites in stratum radiatum (SR), relatively close to the soma. EC LII(3) and LIII(6) pyramidal neuron axons provide direct, but weak, excitatory drive by forming synapses on regions of the CA1 pyramidal neuron apical dendrites located in stratum lacunosum moleculare (SLM), very far from the soma. Both indirect and direct inputs also recruit strong feedforward inhibition (FFI) that normally limits CA1 excitation(7).

Previous studies have demonstrated that coordinated activation of the direct and trisynaptic inputs to CA1 pyramidal neurons enhances the propagation of excitatory postsynaptic potentials (EPSPs) along the pyramidal neuron apical dendrites(8), enables the firing of dendritic spikes and bursts of action potential output(9), induces a robust and temporally precise form of heterosynaptic plasticity (termed input timing dependent plasticity or ITDP) (10, 11), and leads to de novo place cell firing (12). However, the contribution of the LRIPs to corticohippocampal activity has not been previously investigated. Here we have characterized the activity of the LRIPs *in vivo*, analyzed their role in long-term memory storage, and investigated their function in regulating the effects of paired EC and CA3 input, in particular CA1 pyramidal neuron synaptic activation, dendritic spike firing, and the induction of heterosynaptic plasticity.

Lateral entorhinal cortex provides direct GABAergic inhibition to local CA1 interneurons

LRIPs from superficial layers of medial entorhinal cortex (MEC), an area that encodes spatial information(13, 14), form synapses with inhibitory neurons (INs) located near the SR/SLM border of the CA1 region(4). However, the LRIPs from MEC are sparse and generate relatively weak inhibitory postsynaptic currents (IPSCs) in the CA1 border INs (4). To determine whether lateral entorhinal cortex (LEC), which conveys multimodal non-spatial sensory information to hippocampus(15), sends a more potent inhibitory projection to CA1 border INs, we injected recombinant Cre-dependent adeno-associated viral vectors (rAAV^{Cre}) into LEC or MEC to label the LRIPs and achieve optogenetic control of their activity. To restrict expression to INs, viral injections were performed using a pan GABAergic Cre-driver mouse line (GAD2-Cre mice(16)) (Fig. 1A; fig. S1).

Injections of two separate rAAV^{Cre} vectors were used to express tdTomato in LEC and GFP in MEC. In contrast to the relatively weak and sparse inhibitory projections from MEC(4), LEC sent dense projections to CA1 (Fig. 1 B–E; fig. S1) that covered twice the area in CA1 ($82.05 \pm 3.64\%$) as do the LRIPs from MEC ($37.79 \pm 2.35\%$; $P < 0.0001$, two-tailed t-test, $n = 5$ mice, fig. S2). Similar to their glutamatergic counterparts, LRIPs from MEC differentially targeted CA1 along its transverse, proximal-distal axis (CA2 side to subiculum side), showing starkly denser projections to proximal regions of CA1 (i.e., those closer to CA2; fig. S2). In contrast to the preferential targeting of LEC excitatory inputs to distal CA1

(closer to subiculum), LRIPs from LEC were distributed fairly uniformly along the proximal-distal axis of CA1 with also a small but significant bias towards the proximal side (fig. S2, S6).

To examine the functional impact of these inputs, we injected an rAAV^{cre} vector in LEC or MEC of GAD2-Cre mice, which enabled us to express ChR2-EYFP(17) selectively in GABAergic neurons in either region. Photostimulation of ChR2-EYFP⁺ GABAergic axons from LEC in the CA1 SLM region in hippocampal slices (Fig. 1C) evoked large inhibitory postsynaptic currents (IPSCs) in CA1 SR/SLM interneurons voltage-clamped to +10 mV (139 ± 24.8 pA, n = 17 responsive cells; Fig. 1F,G). In contrast, the IPSCs evoked by photostimulation of ChR2-EYFP⁺ MEC LRIPs were only one fourth as large (37.7 ± 4.5 pA, n = 11 responsive cells; P < 0.005, t-test; Fig. 1F,G). Moreover, a greater fraction of SR/SLM INs responded to photostimulation of LEC LRIPs (53.4%) compared to MEC LRIPs (32.4%; fig. S3B).

These synaptic currents were eliminated by the GABA_A and GABA_B receptor blockers SR 95531 (2 μM) and CGP-54626 (1 μM), respectively, but were unaltered by blockade of AMPA-type glutamate receptors (NBQX 10 μM), indicating that the responses represented direct IPSCs generated by GABA release from the LRIPs (Fig. 1F; fig. S3C). We failed to detect any EPSPs in CA1 SR/SLM INs when we photostimulated ChR2-YFP+ LEC axons under current clamp conditions with the INs held at an initial membrane potential of -68 mV (fig. S3D), indicating that the rAAV^{cre} vector resulted in the selective expression of ChR2 in LEC GABAergic neurons.

LRIPs regulate the precision of memory storage

As LEC conveys non-spatial contextual information, we reasoned that the LRIP inputs may be important for non-spatial forms of learning, including contextual fear conditioning (CFC) (18), a hippocampal-dependent form of memory. We therefore examined the effect of silencing the LRIPs on CFC using the engineered ligand-gated glycine receptor, PSAM (Pharmacogenetically Selective Actuator Module), which powerfully inhibits neural activity upon binding its cognate synthetic ligand PSEM³⁰⁸ (Pharmacogenetically Selective Effector Module)(11, 19). To selectively silence the LEC LRIPs in CA1 without altering inhibition in EC, we implanted bilateral cannulae to locally infuse PSEM (15 μM, PSEM³⁰⁸) in dorsal CA1 of Gad2-Cre mice expressing either GFP (control) or PSAM (test) as a result of rAAV^{Cre} injections in LEC (Fig. 2A–B; figs. S4, S5). We verified that the local infusion selectively targeted LRIPs in hippocampus and spared EC by examining the distribution of the dye miniRuby (5%), which was present in the PSEM infusate (fig. S4, S5). PSEM³⁰⁸ infusion did not alter locomotor activity or cause anxiety-like behavior, indicating that the drug infusion did not have significant adverse effects (fig. S7).

To test if the LRIPs were required for CFC, we infused PSEM just prior to the training phase on day 1 of the CFC task, in which the mice were placed in a novel context A for 2.5 min, followed by a brief, aversive foot shock (Fig. 2C, see Methods)(20). When placed in the training environment (context A) 24 hours after training (day 2, no PSEM present), the control (GFP-expressing) group demonstrated fear learning, as assessed by increased

freezing behavior (Fig. 2D). However, rather than inhibiting CFC, silencing of the LEC LRIPs during training on day 1 significantly increased freezing on day 2 in context A ($37.7 \pm 2.3\%$, GFP, $n = 9$; $53.23 \pm 2.7\%$, PSAM, $n = 7$; $P < 0.0001$, Two-way ANOVA; $P = 0.0007$, t-test, two tailed paired by time; Fig. 2D), demonstrating that the LRIPs were not necessary for contextual learning.

However, when we exposed the mice on day 3 of the task to a novel context B, designed to be readily distinguishable from context A, the two groups of mice showed a revealing difference. Whereas the control mice did not freeze in the novel context, reflecting the normal specificity of CFC to the training context, the PSAM-expressing test group (where the LRIPs were only silenced during training in context A on day 1) exhibited a significant level of inappropriate freezing to the novel context (GFP: $5.1 \pm 3.9\%$, $n = 9$; PSAM: $21.1 \pm 7.9\%$, $n = 7$; $P = 0.018$, Two-way ANOVA; $P = 0.0446$, two-tailed t-test paired by time; Fig. 2D). The freezing to the novel context B in the test group was also significantly greater than the amount of freezing in context A prior to training ($P < 0.0002$), suggesting that the freezing represented an inappropriately learned response that caused an overgeneralization of fear memory. In contrast, the control group showed similar, low levels of freezing to context A on day 1 and context B on day 3 ($P > 0.5$). Finally, the difference in fear learning was specific for hippocampal-dependent CFC and did not reflect a general increase in fear or anxiety because the two groups of mice displayed similar extents of amygdala-dependent cued fear conditioning to a tone paired with the footshock (Fig. 2D).

We next tested the importance of the LRIPs in a second non-spatial memory task, novel object recognition, using a version of the task that is hippocampal-dependent (21–25) (Fig. 2E). Mice were exposed to two objects during two 10-min training trials. After a 10-minute delay, one of the now-familiar objects was substituted for a novel object, and the time spent exploring the novel versus familiar object was determined. The control group explored the old object for 25.62 ± 4.26 s and the new object for 66.33 ± 13.5 s ($n = 6$; $P < 0.05$, paired t-test), indicating object recognition memory. Similar to CFC, the LRIPs were not required for object memory storage as mice treated with PSEM during the training trials explored the novel object for a significantly longer time (86.38 ± 7.49 s) than they explored the familiar object (49.38 ± 3.55 s; $n = 6$; $P < 0.05$, paired t-test) (Fig. 2F). However, the LRIPs were required for optimal memory storage, as the degree of memory performance, measured by the discrimination index for the two objects (Fig. 2G, see legend), was significantly greater for control (0.52 ± 0.06 ; $n = 6$) versus PSEM-treated mice (0.29 ± 0.06 ; $P < 0.05$, paired t-test). Interestingly, PSEM treatment also decreased the habituation that mice normally show to the objects during the second of the two training trials (fig. S7; $P < 0.005$). Thus, while the LRIPs were not necessary for memory storage in two separate hippocampal-dependent non-spatial memory tasks, these inputs were important for enhancing the specificity of memory associations in performance of the two tasks.

LEC GABAergic inputs to CA1 are activated by sensory, motivational and aversive stimuli *in vivo*

To explore how the LRIPs encode signals that might contribute to performance of non-spatial memory tasks, we used Ca^{2+} imaging to examine the responses of these inputs to a variety of sensory cues. We injected rAAV^{Cre} in LEC of GAD2-Cre mice to express the genetically encoded Ca^{2+} indicator GCaMP6f(26) in GABAergic neurons. *In vivo* two-photon microscopy was then used to image Ca^{2+} signals in LRIP axons and axon terminals in the CA1 SLM region in response to a light stimulus, tone, aversive airpuff or water reward (Fig. 3A–C) as described(27, 28).

The sensory and behaviorally relevant stimuli elicited transient Ca^{2+} signals in LRIP axons and presynaptic boutons (Fig. 3D–F), with the aversive airpuff eliciting the largest response ($F/F = 0.55 \pm 0.05$) and greatest percentage of responsive boutons (22.9%). This result is of interest as the aversive airpuff is capable of serving as the unconditioned stimulus in a head-fixed CFC protocol(28). Water reward elicited a comparable Ca^{2+} signal in responsive boutons ($F/F = 0.58 \pm 0.07$, Video S1), but only half as many boutons responded (11.9%) as compared to the airpuff.

As environmental contexts are comprised of multi-sensory modalities, we also examined LRIP responses to pairs of stimuli (Fig. 3G). Paired stimuli tended to evoke larger Ca^{2+} responses in a greater fraction of boutons than did single stimuli. Pairing tone or light with airpuff led to a 1.4-, 2.0- and 3.2-fold greater Ca^{2+} response than when airpuff, tone or light were presented alone, respectively, with a 2–8 fold increase in the fraction of active boutons (Fig. 3H–J). Whereas individual boutons usually responded to at most one or two of the four individual stimuli, collectively the LRIPs were able to represent the four sensory modalities examined (fig. S8D). Moreover, the probability that a single bouton responded to 3 distinct pairs of stimuli was higher than predicted from a random, independent distribution of boutons based on the measured response to individual pairs of stimuli. Thus, a subpopulation of LRIPs may be specifically tuned to encode multimodal sensory cues, similar to what constitutes a behavioral context.

Spontaneous motor behaviors, such as spontaneous running and licking, also elicited Ca^{2+} responses in the LRIPs (fig. S8E). Although the aversive airpuff typically elicited a running response, the airpuff recruited a greater fraction of boutons and evoked a larger Ca^{2+} signal compared to that seen with spontaneous running, indicating a specific sensory contribution to the airpuff response. Furthermore, LRIP boutons that made apparent contacts on dendrites had larger Ca^{2+} responses than did boutons that targeted SR/SLM interneuron somata (fig. S8F,G).

We wondered as to why different boutons showed such diverse responses to different stimuli. One clue came from the finding that boutons along a single axon responded more uniformly to a set of sensory cues than did neighboring boutons from different fibers (fig. S8H,I). This indicated that the variability in bouton response was likely not caused by random trial-to-trial variability but rather resulted from the specific tuning of individual LRIP axons to distinct combinations of sensory and behavioral cues. This finding is

consistent with the idea that these inputs are important for regulating non-spatial contextual and object memory.

LRIPs from LEC transiently inhibit spike output of local CA1 dendritetargeting feed-forward inhibitory neurons

How do the long-range GABAergic projections influence information flow through the cortico-hippocampal circuit to regulate memory storage? We began to investigate this question by performing whole cell recordings from cholecystokinin-positive (CCK+) SR/SLM interneurons, which represent a large fraction of the SR/SLM border INs targeted by the LRIPs (fig. S9). Moreover, the CCK+ INs receive strong excitatory drive from the Schaffer collaterals and send strong inhibitory output to CA1 pyramidal neuron dendrites(11, 29, 30).

To determine how the CCK+ INs integrate their cortical and hippocampal inputs, we electrically stimulated the SC axons (using an electrode in SR) or a mixed population of excitatory and inhibitory EC axons (using an electrode in SLM). We then recorded the synaptic responses in genetically-defined CCK⁺ SR/SLM INs tagged with GFP(11, 16) (Fig. 4A–C). These neurons displayed a large voltage sag in response to hyperpolarization and an intermediate firing pattern, characteristic of CCK INs (29, 31–33) (Fig. 4D).

SC stimulation elicited a strongly depolarizing PSP in the CCK+ INs, with a peak amplitude of 9.83 ± 0.17 mV at 50% maximal stimulation strength (Fig. 4E). In contrast, EC stimulation evoked a mixed EPSP/IPSP (peak depolarization = 0.79 ± 0.34 mV) that was dominated by a large hyperpolarization, which reached its peak negative value (-5.59 ± 0.17 mV, n = 7) approximately 20 ms after the stimulus (Fig. 4F). As we show below, the time course of the hyperpolarization imposes a precise timing-dependence for disinhibition, which regulates the timing of the induction of ITDP (Fig. 7) and the generation of dendritic spikes (Fig. 8) in response to paired stimulation of the EC and SC inputs. The EC-evoked IPSP was unaffected by blockers of glutamatergic transmission (NBQX 10 μ M; AP-V 100 μ M), demonstrating it resulted from direct activation of GABAergic axons rather than disynaptic FFI (Fig. 4F).

To determine whether the electrically-evoked IPSP was caused by GABA release from the LRIPs, we silenced these projections using the PSAM/PSEM approach (Fig. 4G,H). Two independent rAAV^{Cre} vectors expressing ChR2 and PSAM were injected into LEC and MEC of Gad2-Cre mice (Fig. 4G). The light-evoked IPSC recorded from SR/SLM INs was fully blocked by local bath application of 3–5 μ M PSEM³⁰⁸ (IPSC = 0.013 ± 0.04 pA, n = 11), verifying the efficacy of this method (Fig. 4I). Silencing the LRIPs nearly abolished the hyperpolarizing component of the mixed PSP evoked by electrical stimulation (peak negative value reduced to -0.29 ± 0.21 mV, n = 7) while it increased the peak depolarization during the PSP (to 4.79 ± 0.79 mV), demonstrating the importance of this projection. PSEM caused no change in the hyperpolarizing or depolarizing components of the PSP evoked by electrical stimulation of the SC axons in SR (Fig. 4J), indicating the specificity of the approach.

How does LRIP activation affect action potential output of the SR/SLM INs in response to paired stimulation of their EC and SC inputs? Electrical stimulation of the EC pathway alone failed to trigger spike firing (Fig. 4K), consistent with the weak depolarizing phase of the mixed EPSP/IPSP response (Fig. 4F). In contrast, moderately strong stimulation of the SC pathway alone (50 μ A stimulus) elicited a large depolarizing PSP that triggered a spike in SR/SLM INs with >50% probability (Fig. 4L). However, when the SC stimulus was preceded by a stimulus to the EC inputs that occurred precisely 15–20 ms before stimulation of the SC inputs, the ability of the SC inputs to trigger action potentials in the SR/SLM INs was suppressed (Fig. 4K,L). The timing-dependence of spike suppression coincided with the maximal hyperpolarization of the SR/SLM INs in response to EC stimulation, suggesting that the suppression of spike firing was mediated by the activation of the LRIP inputs. Consistent with this idea, silencing the LRIPs with PSAM/PSEM prevented the suppression of spike firing upon electrical stimulation of the EC inputs (Fig. 4K,L).

LRIPs provide a temporally precise gate of hippocampal input to CA1

What are the consequences of the LRIP-mediated suppression of SR/SLM IN firing for the activity of CA1 pyramidal neurons? To examine this question, we virally expressed ChR2 in CCK⁺ INs in the CA1 SLM region and measured the light-evoked IPSC in CA1 PNs voltage-clamped at +10 mV (Fig. 5A–B). Photostimulation of the CCK⁺ INs using a light pulse focused in SR produced a robust IPSC in the CA1 PN soma (~250 μ m from the light spot). Electrical stimulation of the EC inputs 20 ms prior to photostimulation significantly suppressed the light-evoked IPSC (to $75.6 \pm 2.7\%$ of the unpaired light-evoked IPSC, $n = 9$; $P < 0.0001$, Two-way ANOVA; Fig. 5C–E), with little change at other pairing intervals. Electrical stimulation did not alter the light-evoked IPSC when ChR2-EYFP was expressed in parvalbumin-positive (PV+) INs, regardless of pairing interval, indicating the specificity of the effect. As ChR2 photostimulation provides an unusually strong excitatory drive compared to an action potential, the LRIPs are likely to produce an even greater suppression of the CCK⁺ IN-mediated IPSP evoked by excitatory synaptic input.

Does the suppression of CCK⁺ IN firing by the LRIPs influence the ability of the EC or SC inputs to excite CA1 PNs? As the SR/SLM INs are known to target CA1 PN apical dendrites, we addressed this question using whole cell recordings from CA1 PN dendrites in SR during single or paired stimulation of the EC and SC inputs (Fig. 6).

Stimulation of the SC input alone evoked a large depolarizing PSP in the proximal dendrite ~150 μ m from the soma (4.48 ± 0.57 mV; fig. S10, $n = 5$).

Stimulation of the EC input alone evoked only a very small dendritic depolarization (1.00 ± 0.24 mV, fig. S10). However, when we stimulated the EC input 20 ms prior to the SC input, we observed a supralinear boosting of dendritic depolarization (Fig. 6B,C), resulting in a net PSP that was 1.35 ± 0.02 fold greater than the PSP evoked by stimulation of the SC pathway alone (significantly greater than the predicted linear sum of 1.13 ± 0.024 fold the SC response alone; $P < 0.05$, t-test; $n = 5$). Paired EC-SC stimulation at the –20 ms interval was associated with an even greater 2.2-fold increase in the postsynaptic Ca²⁺ transient in

CA1 PN dendritic spines in SR, relative to the Ca^{2+} transient elicited by SC input alone (fig. S10; $P < 0.001$, t-test, $n = 5$).

Strikingly, the supralinear boosting was sharply tuned to the -20 ms pairing interval. Paired activation of EC and SC inputs at other intervals resulted in linear or sublinear summation (Fig. 6B,C). Moreover, pairing at the -10 ms interval produced a significantly lower boosting in spine Ca^{2+} compared to the -20 ms interval (1.3-fold, $P < 0.0001$, t-test, $n = 5$).

The timing-dependence of the supralinear boosting of the CA1 PN PSP suggested to us that it might result from a disinhibitory action of the LRIPs to suppress SC-evoked FFI through the SR/SLM INs (Fig. 6D). We therefore compared the effect of paired EC-SC stimulation before and after application of GABAR antagonists (Fig. 6B,C). Blockade of inhibition greatly increased the peak depolarization during the PSP evoked by stimulation of the EC and/or SC inputs, reflecting the removal of FFI (Fig. 6B, fig. S10B,C). Of note, paired EC-SC stimulation produced only a linear or sublinear summation at all pairing intervals in the presence of the antagonists, consistent with the view that supralinear summation was caused by disinhibition. For example, pairing at a -10 ms interval resulted in a net PSP 1.19 ± 0.06 fold larger than the SC PSP alone, and not significantly different from the linear sum of the EC+SC PSPs ($P = 0.238$). In addition, the peak of the paired response was shifted to the -10 ms pairing interval, which corresponds to the expected peak of temporal summation of the individual EC and SC EPSPs.

Next, we tested directly whether the LRIPs were responsible for the supralinear boosting by recording PSPs in distal CA1 PN dendrites (300 μm from the soma) in response to paired EC-SC stimulation, before and after silencing the LRIPs (Fig. 6D–F). We found that application of PSEM³⁰⁸ (3 μM) to slices in which the LRIPs expressed PSAM fully prevented the supralinear boosting (Fig. 6E,F). Thus, we propose that the EC LRIPs potentiate the ability of the SC inputs to excite CA1 pyramidal neuron dendrites by suppressing SC-evoked feedforward inhibition mediated by the SR/SLM interneurons.

Disinhibition through LEC LRIPs enables input-timing-dependent plasticity and dendritic spike firing

Given the behavioral role of the LRIPs in memory storage, we asked whether these inputs may also contribute to more robust, longer-lasting forms of SC input gating than the transient boosting of dendritic depolarization and spine Ca^{2+} levels seen above. Paired EC-SC stimulation at 1 Hz for 90 s induces a long-lasting form of heterosynaptic plasticity, termed input-timing-dependent plasticity (ITDP), that strongly enhances SC-evoked excitation of the CA1 PN(10, 11). As the induction of ITDP is finely tuned to the same -20 ms pairing interval optimal for LRIP-mediated disinhibition, we hypothesized that the LRIPs from EC may be required for this plasticity. In support of this view, we found that silencing of PSAM-expressing LRIPs, either from LEC alone or from both LEC and MEC, with PSEM³⁰⁸ fully blocked the induction of ITDP (Fig. 7A,B).

The above results suggest that the induction of ITDP is normally suppressed by FFI evoked by SC stimulation, and thus requires LRIP activation to suppress this inhibition. This model

would also explain how the induction of ITDP is finely tuned to the -20 ms pairing interval. This scenario predicts that robust ITDP may be induced over a broader range of pairing intervals in the presence of GABAR antagonists, which would eliminate FFI at all pairing intervals. Consistent with this model, we found that the presence of GABAR blockers during the ITDP induction protocol alone enabled the induction of robust ITDP over a broader range of pairing intervals, from -10 to -30 ms (Fig. 7I). This ITDP tuning curve now matched the expected time course of temporal summation of the EC and SC EPSPs (10).

How could the relatively modest boosting by the LRIPs of the EC-SC synaptic depolarization lead to such a robust form of plasticity? Many forms of long-term synaptic plasticity that do not depend on somatic action potentials (such as ITDP (10, 11)) require the firing of dendritic spikes, which can enhance Ca^{2+} influx into the postsynaptic cell (34, 35). Thus, we next examined whether more prolonged EC-SC pairing, as used to induce ITDP, promoted dendritic spiking, using whole cell recordings from distal CA1 PN dendrites (~300 μm from the soma, Fig. 8A).

Although single paired EC-SC stimulation failed to elicit a dendritic spike, large regenerative spikes began to appear when we delivered 10 or more paired EC-SC stimuli at 1 Hz using a -20 ms interval (Fig. 8B). Event amplitude frequency histograms (Fig. 8C) showed three peaks, corresponding to subthreshold PSPs (~20 mV amplitude), small brief action potentials (~40 mV) resembling dendritic Na^+ spikes(34), and longer, larger events (~60 mV) resembling dendritic Ca^{2+} spikes(36, 37). Both types of spikes were preferentially generated at the -20 ms pairing interval compared to a -10 ms pairing interval. Both types of spikes also required LRIP input as spike probability greatly decreased when the LEC LRIPs were silenced with PSAM/PSEM (Fig. 8D-F).

Experiments using two-photon Ca^{2+} imaging in CA1 PNs supported the view that the dendritic spikes may contribute to the induction of ITDP. Repetitive stimulation of EC-SC inputs at 1 Hz using a -20 ms pairing interval led to longlasting Ca^{2+} signals in the apical dendrites that propagated to the soma (fig. S10F-G). These dendritic signals provide a likely source for the intracellular Ca^{2+} required for the induction of ITDP (10, 11). Pairing-induced dendritic spikes gated by the LRIPs may thus provide a powerful non-linear mechanism for the longterm enhancement of SC-mediated excitation in response to temporally precise, coordinated cortico-hippocampal dendritic activity.

Discussion

The importance of excitatory projections from lateral and medial entorhinal cortex to hippocampus for memory storage and spatial encoding is well established(38). MEC also sends LRIPs to hippocampus that form synapses on CA1 SR/SLM GABAergic interneurons(4), although the *in vivo* function of these inputs was not determined. Here we report that LEC sends LRIPs to CA1 that exert an even stronger inhibitory drive on CA1 SR/SLM INs compared to the LRIPs from MEC. We also found that LRIPs from LEC convey multimodal sensory information that helps fine-tune the specificity of hippocampal dependent contextual memory storage and enhances the ability to distinguish novel from familiar objects. Finally the LRIPs provide a temporally precise disinhibitory gating

mechanism for enhancing information flow within the hippocampal circuit at both short and long time scales.

Within the context of the cortico-hippocampal circuit, the LRIPs transiently suppress dendritic feedforward inhibition to enhance excitatory signals from the trisynaptic path that arrive at CA1 PNs precisely 20 ms after LRIP activation. The effect of this disinhibitory gating has ramifications across widely different time scales. Activation of the LRIPs with a single pairing of EC-SC stimulation at a -20 ms interval causes a transient supralinear boost in local dendritic depolarization and proximal spine Ca^{2+} . Repetitive paired stimulation of EC and SC inputs at the same interval leads to further amplification of synaptic input by promoting the firing of dendritic spikes (9, 36) and the induction of ITDP, a robust Ca^{2+} -dependent form of long-term heterosynaptic plasticity (10, 11). Given that dendritic spikes are normally suppressed by strong feedforward inhibition(9), the ability of the LRIPs to enhance dendritic spiking during a precise temporal window may contribute to the dendritic spike firing *in vivo* observed during behaviorally relevant cooperative activity(39). The LRIP-dependent dendritic spikes are likely to participate in the induction of ITDP and the fine-tuning of learning and memory, based on the role of such spikes in both other forms of Ca^{2+} -dependent synaptic plasticity(35, 36, 40) and non-linear gain modulation during associative learning(35) and sensory tuning(41).

Our findings, together with previous results(28, 42) (43–45), further demonstrate how distinct populations of local interneurons play well-defined roles in hippocampal dependent behaviors and circuit function. We found that CCK⁺ INs located near the SR/SLM border exert strong FFI onto CA1 PN dendrites; LRIP-mediated transient suppression of these INs enables temporally precise supralinear dendritic excitation. The GABAR kinetics, CA1 pyramidal neuron membrane time constant(29);(46), and *in vivo* firing patterns(47) of the CCK⁺ INs are all likely to participate in ensuring that the kinetics of the LRIP-mediated IPSP are appropriately tuned to implement the 20-ms gating of information flow from the SC inputs to CA1 PNs. Of note, mice have been found to display an over-generalized contextual learning phenotype upon perturbation of signaling in CA1 CCK⁺ INs(48), similar to our behavioral findings upon silencing the LRIPs that target these INs.

The role of the CCK⁺ SR/SLM border INs in implementing the ITDP timing rule contrasts with the role in ITDP of a separate subclass of CCK⁺ INs, the perisomatic targeting basket cells located in and around the CA1 PN cell body layer(11). Previously we found that the expression of ITDP results from the combined effects of long-term potentiation of the SC excitatory synapses on CA1 pyramidal neurons and the long-term depression of FFI from a population of perisomatic CCK INs onto the same CA1 pyramidal cells(11). Thus, anatomically distinct subpopulations of the same genetically-defined class of CCK⁺ INs are specifically involved in the induction versus the expression of ITDP. Yet another class of CA1 INs, the somatostatin-positive dendrite targeting INs, has been found to be required for CFC(28). These INs serve to suppress EC input to CA1 PN dendrites during aversive stimuli, thereby ensuring that the unconditioned stimulus is not encoded as part of the contextual representation. Thus, distinct populations of GABAergic INs participate in distinct microcircuits to regulate separate phases of memory encoding.

What is the significance of the precise 20 ms temporal window for LRIP-dependent disinhibitory gating? One interesting possibility is suggested by the fact that this interval is matched to the dynamics of the delay-line architecture of the cortico-hippocampal circuit, where signals propagating through the trisynaptic path arrive at CA1 PNs approximately 15–20 ms after the arrival of signals through the direct path(49). Thus, the temporal dynamics of LRIP-mediated disinhibition will enhance the propagation to a given CA1 pyramidal neuron of those signals arriving through the trisynaptic path that were initiated by activity in EC LII stellate cells (which project to dentate gyrus) simultaneously with activity in the subset of EC LII(3) and LIII pyramidal neurons(6) that directly project to the same CA1 pyramidal neuron. This timing rule for disinhibitory gating may therefore serve as a filter to assess the salience of processed associations arriving from CA3 inputs based on their temporal relation to the direct multimodal sensory inputs arriving from EC.

Because our studies of the effects of LRIP activation on CA1 PN function were carried out in *ex vivo* hippocampal slices, a key question is whether the 20 ms timing interval between cortical and SC input that is required for the boosting of SC excitation is implemented by *in vivo* patterns of cortico-hippocampal activity. Studies of the temporal relation of oscillatory activity in entorhinal cortex and hippocampus *in vivo* suggest that the disinhibitory gating mechanism may indeed be engaged during spatial behavior(50, 51) and associational learning(52). For example, during running and memory tasks, fast gamma oscillations (100 Hz) arising from EC LIII are observed in SLM of CA1 and precede the slow gamma oscillations (50 Hz) in SR of CA1, which are thought to reflect CA3 pyramidal neuron input(50). Importantly, EC LIII–CA1 gamma activity and CA3-CA1 gamma activity display a 90° phase offset during theta frequency oscillations (8–9 Hz)(50) that is consistent with a ~20–25 ms time delay.

Learning is a critical adaptive behavior and the precision of memory storage normally enables an animal to discriminate between harmful (salient) versus safe (neutral) environments. Failure to do so can lead to overgeneralization of fear memories, a characteristic feature of post-traumatic stress and other anxiety disorders. How might the effect of the LRIPs to enhance cortico-hippocampal information flow contribute to their behavioral role to enhance learning specificity? The increased freezing in the conditioned and novel contexts upon silencing the LRIPs indicates that the disinhibitory circuit, and by implication ITDP, is not required for generalized fear learning, which may be implemented by other intra-hippocampal circuits(28, 53) or other forms of plasticity, such as SC Hebbian LTP. Similarly, the LRIPs are not needed for basic object recognition memory. Rather, we suggest that the LRIPs may enhance contextual and object memory storage and improve memory specificity by creating a sparse, high-contrast ensemble of potentiated SC synapses whose dynamics conform to the temporal window of paired EC-SC associative inputs that enables the induction of ITDP.

Supplementary Material

Refer to Web version on PubMed Central for supplementary material.

Acknowledgments

We thank Karl Deisseroth, Scott Sternson, Z. Josh Huang and Gordon Fishell for generously sharing reagents and transgenic mice. We are grateful to Gyorgy Buzsaki, Richard Tsien, Rene Hen, Alex Dranovsky, Christoph Kellendonk, Stefano Fusi, Randy Bruno and Aniruddha Das for invaluable discussions on the study and Chris Magnus, Scott Sternson, Christine Denny, Aaron Katzman and Marco Russo for critical technical advice. We are also indebted to Justine Kupferman, Zev Rosen, Arjun Masurkar, Qian Sun and Tobias Bock for helpful comments on previous versions of the manuscript. This work was supported by a NARSAD Young Investigator grant to JB; a Ruth L. Kirschstein F30 NRSA NIMH to FLH; a Human Frontier Science Program grant and a grant from NIH/NIMH (1R01MH100510) to BVZ; a grant from NIH/NIMH (1R01MH100631) and support from the Searle Scholars Program, Human Frontier Science Program and the McKnight Memory and Cognitive Disorders Award to AL; and a grant from NIH/NINDS (R01NS036658) and support from the Howard Hughes Medical Institute to SAS.

References and Notes

1. Brun VH, et al. Impaired spatial representation in CA1 after lesion of direct input from entorhinal cortex. *Neuron*. 2008; 57:290–302. [PubMed: 18215625]
2. Suh J, Rivest AJ, Nakashiba T, Tominaga T, Tonegawa S. Entorhinal cortex layer III input to the hippocampus is crucial for temporal association memory. *Science*. 2011; 334:1415–1420. [PubMed: 22052975]
3. Kitamura T, et al. Island cells control temporal association memory. *Science*. 2014; 343:896–901. [PubMed: 24457215]
4. Melzer S, et al. Long-range-projecting GABAergic neurons modulate inhibition in hippocampus and entorhinal cortex. *Science*. 2012; 335:1506–1510. [PubMed: 22442486]
5. Amaral DG, Witter MP. The three-dimensional organization of the hippocampal formation: a review of anatomical data. *Neuroscience*. 1989; 31:571–591. [PubMed: 2687721]
6. Witter MP, Amaral DG. Entorhinal cortex of the monkey: V. Projections to the dentate gyrus, hippocampus, and subiculum complex. *The Journal of comparative neurology*. 1991; 307:437–459. [PubMed: 1713237]
7. Buzsaki G. Feed-forward inhibition in the hippocampal formation. *Progress in neurobiology*. 1984; 22:131–153. [PubMed: 6433403]
8. Jarsky T, Roxin A, Kath WL, Spruston N. Conditional dendritic spike propagation following distal synaptic activation of hippocampal CA1 pyramidal neurons. *Nature neuroscience*. 2005; 8:1667–1676. [PubMed: 16299501]
9. Takahashi H, Magee JC. Pathway interactions and synaptic plasticity in the dendritic tuft regions of CA1 pyramidal neurons. *Neuron*. 2009; 62:102–111. [PubMed: 19376070]
10. Dudman JT, Tsay D, Siegelbaum SA. A role for synaptic inputs at distal dendrites: instructive signals for hippocampal long-term plasticity. *Neuron*. 2007; 56:866–879. [PubMed: 18054862]
11. Basu J, et al. A cortico-hippocampal learning rule shapes inhibitory microcircuit activity to enhance hippocampal information flow. *Neuron*. 2013; 79:1208–1221. [PubMed: 24050406]
12. Bittner KC, et al. Conjunctive input processing drives feature selectivity in hippocampal CA1 neurons. *Nature neuroscience*. 2015; 18:1133–1142. [PubMed: 26167906]
13. Brun VH, et al. Place cells and place recognition maintained by direct entorhinal-hippocampal circuitry. *Science*. 2002; 296:2243–2246. [PubMed: 12077421]
14. Fyhn M, Molden S, Witter MP, Moser EI, Moser MB. Spatial representation in the entorhinal cortex. *Science*. 2004; 305:1258–1264. [PubMed: 15333832]
15. Hargreaves EL, Rao G, Lee I, Knierim JJ. Major dissociation between medial and lateral entorhinal input to dorsal hippocampus. *Science*. 2005; 308:1792–1794. [PubMed: 15961670]
16. Taniguchi H, et al. A resource of Cre driver lines for genetic targeting of GABAergic neurons in cerebral cortex. *Neuron*. 2011; 71:995–1013. [PubMed: 21943598]
17. Boyden ES, Zhang F, Bamberg E, Nagel G, Deisseroth K. Millisecond-timescale, genetically targeted optical control of neural activity. *Nature neuroscience*. 2005; 8:1263–1268. [PubMed: 16116447]
18. Maren S, Phan KL, Liberzon I. The contextual brain: implications for fear conditioning, extinction and psychopathology. *Nature reviews Neuroscience*. 2013; 14:417–428. [PubMed: 23635870]

19. Magnus CJ, et al. Chemical and genetic engineering of selective ion channel-ligand interactions. *Science*. 2011; 333:1292–1296. [PubMed: 21885782]
20. Hitti FL, Siegelbaum SA. The hippocampal CA2 region is essential for social memory. *Nature*. 2014; 508:88–92. [PubMed: 24572357]
21. Cohen SJ, Stackman RW Jr. Assessing rodent hippocampal involvement in the novel object recognition task. A review. *Behavioural brain research*. 2015; 285:105–117. [PubMed: 25169255]
22. Clark RE, Zola SM, Squire LR. Impaired recognition memory in rats after damage to the hippocampus. *The Journal of neuroscience : the official journal of the Society for Neuroscience*. 2000; 20:8853–8860. [PubMed: 11102494]
23. Ainge JA, et al. The role of the hippocampus in object recognition in rats: examination of the influence of task parameters and lesion size. *Behavioural brain research*. 2006; 167:183–195. [PubMed: 16214239]
24. Cohen SJ, et al. The rodent hippocampus is essential for nonspatial object memory. *Current biology : CB*. 2013; 23:1685–1690. [PubMed: 23954431]
25. Denny CA, Burghardt NS, Schachter DM, Hen R, Drew MR. 4- to 6-week-old adult-born hippocampal neurons influence novelty-evoked exploration and contextual fear conditioning. *Hippocampus*. 2012; 22:1188–1201. [PubMed: 21739523]
26. Chen TW, et al. Ultrasensitive fluorescent proteins for imaging neuronal activity. *Nature*. 2013; 499:295–300. [PubMed: 23868258]
27. Kaifosh P, Lovett-Barron M, Turi GF, Reardon TR, Losonczy A. Septo-hippocampal GABAergic signaling across multiple modalities in awake mice. *Nature neuroscience*. 2013; 16:1182–1184. [PubMed: 23912949]
28. Lovett-Barron M, et al. Dendritic inhibition in the hippocampus supports fear learning. *Science*. 2014; 343:857–863. [PubMed: 24558155]
29. Cope DW, et al. Cholecystokinin-immunopositive basket and Schaffer collateral-associated interneurones target different domains of pyramidal cells in the CA1 area of the rat hippocampus. *Neuroscience*. 2002; 109:63–80. [PubMed: 11784700]
30. Klausberger T, Somogyi P. Neuronal diversity and temporal dynamics: the unity of hippocampal circuit operations. *Science*. 2008; 321:53–57. [PubMed: 18599766]
31. Pawelzik H, Hughes DI, Thomson AM. Physiological and morphological diversity of immunocytochemically defined parvalbumin-and cholecystokinin-positive interneurones in CA1 of the adult rat hippocampus. *The Journal of comparative neurology*. 2002; 443:346–367. [PubMed: 11807843]
32. Lee SH, Soltesz I. Requirement for CB1 but not GABAB receptors in the cholecystokinin mediated inhibition of GABA release from cholecystokinin expressing basket cells. *The Journal of physiology*. 2011; 589:891–902. [PubMed: 21173082]
33. Daw MI, Tricoire L, Erdelyi F, Szabo G, McBain CJ. Asynchronous transmitter release from cholecystokinin-containing inhibitory interneurons is widespread and target-cell independent. *The Journal of neuroscience : the official journal of the Society for Neuroscience*. 2009; 29:11112–11122. [PubMed: 19741117]
34. Golding NL, Spruston N. Dendritic sodium spikes are variable triggers of axonal action potentials in hippocampal CA1 pyramidal neurons. *Neuron*. 1998; 21:1189–1200. [PubMed: 9856473]
35. Gambino F, et al. Sensory-evoked LTP driven by dendritic plateau potentials in vivo. *Nature*. 2014; 515:116–119. [PubMed: 25174710]
36. Golding NL, Staff NP, Spruston N. Dendritic spikes as a mechanism for cooperative long-term potentiation. *Nature*. 2002; 418:326–331. [PubMed: 12124625]
37. Larkum ME, Zhu JJ, Sakmann B. A new cellular mechanism for coupling inputs arriving at different cortical layers. *Nature*. 1999; 398:338–341. [PubMed: 10192334]
38. Buzsaki G, Moser EI. Memory, navigation and theta rhythm in the hippocampal-entorhinal system. *Nature neuroscience*. 2013; 16:130–138. [PubMed: 23354386]
39. Kamondi A, Acsady L, Buzsaki G. Dendritic spikes are enhanced by cooperative network activity in the intact hippocampus. *The Journal of neuroscience : the official journal of the Society for Neuroscience*. 1998; 18:3919–3928. [PubMed: 9570819]

40. Losonczy A, Makara JK, Magee JC. Compartmentalized dendritic plasticity and input feature storage in neurons. *Nature*. 2008; 452:436–441. [PubMed: 18368112]
41. Sheffield ME, Dombeck DA. Calcium transient prevalence across the dendritic arbour predicts place field properties. *Nature*. 2014
42. Royer S, et al. Control of timing, rate and bursts of hippocampal place cells by dendritic and somatic inhibition. *Nature neuroscience*. 2012; 15:769–775. [PubMed: 22446878]
43. Roux L, Buzsaki G. Tasks for inhibitory interneurons in intact brain circuits. *Neuropharmacology*. 2015; 88:10–23. [PubMed: 25239808]
44. Murray AJ, et al. Parvalbumin-positive CA1 interneurons are required for spatial working but not for reference memory. *Nature neuroscience*. 2011; 14:297–299. [PubMed: 21278730]
45. Donato F, Rompani SB, Caroni P. Parvalbumin-expressing basket-cell network plasticity induced by experience regulates adult learning. *Nature*. 2013; 504:272–276. [PubMed: 24336286]
46. Hefft S, Jonas P. Asynchronous GABA release generates long-lasting inhibition at a hippocampal interneuron-principal neuron synapse. *Nature neuroscience*. 2005; 8:1319–1328. [PubMed: 16158066]
47. Klausberger T, et al. Complementary roles of cholecystokinin- and parvalbumin-expressing GABAergic neurons in hippocampal network oscillations. *The Journal of neuroscience : the official journal of the Society for Neuroscience*. 2005; 25:9782–9793. [PubMed: 16237182]
48. Jacob W, Marsch R, Marsicano G, Lutz B, Wotjak CT. Cannabinoid CB1 receptor deficiency increases contextual fear memory under highly aversive conditions and long-term potentiation in vivo. *Neurobiology of learning and memory*. 2012; 98:47–55. [PubMed: 22579951]
49. Yeckel MF, Berger TW. Feedforward excitation of the hippocampus by afferents from the entorhinal cortex: redefinition of the role of the trisynaptic pathway. *Proceedings of the National Academy of Sciences of the United States of America*. 1990; 87:5832–5836. [PubMed: 2377621]
50. Schomburg EW, et al. Theta phase segregation of input-specific gamma patterns in entorhinal-hippocampal networks. *Neuron*. 2014; 84:470–485. [PubMed: 25263753]
51. Chrobak JJ, Lorincz A, Buzsaki G. Physiological patterns in the hippocampo-entorhinal cortex system. *Hippocampus*. 2000; 10:457–465. [PubMed: 10985285]
52. Igarashi KM, Lu L, Colgin LL, Moser MB, Moser EI. Coordination of entorhinal-hippocampal ensemble activity during associative learning. *Nature*. 2014; 510:143–147. [PubMed: 24739966]
53. Nakashiba T, Young JZ, McHugh TJ, Buhl DL, Tonegawa S. Transgenic inhibition of synaptic transmission reveals role of CA3 output in hippocampal learning. *Science*. 2008; 319:1260–1264. [PubMed: 18218862]
54. Hippenmeyer S, et al. A developmental switch in the response of DRG neurons to ETS transcription factor signaling. *PLoS biology*. 2005; 3:e159. [PubMed: 15836427]
55. Madisen L, et al. A robust and high-throughput Cre reporting and characterization system for the whole mouse brain. *Nature neuroscience*. 2010; 13:133–140. [PubMed: 20023653]
56. Miyoshi G, et al. Genetic fate mapping reveals that the caudal ganglionic eminence produces a large and diverse population of superficial cortical interneurons. *The Journal of neuroscience : the official journal of the Society for Neuroscience*. 2010; 30:1582–1594. [PubMed: 20130169]
57. Yamamoto M, et al. A multifunctional reporter mouse line for Cre- and FLP-dependent lineage analysis. *Genesis*. 2009; 47:107–114. [PubMed: 19165827]
58. Zhang F, et al. Optogenetic interrogation of neural circuits: technology for probing mammalian brain structures. *Nature protocols*. 2010; 5:439–456. [PubMed: 20203662]
59. Kupferman JV, et al. Reelin signaling specifies the molecular identity of the pyramidal neuron distal dendritic compartment. *Cell*. 2014; 158:1335–1347. [PubMed: 25201528]
60. Tricoire L, et al. A blueprint for the spatiotemporal origins of mouse hippocampal interneuron diversity. *The Journal of neuroscience : the official journal of the Society for Neuroscience*. 2011; 31:10948–10970. [PubMed: 21795545]
61. Kaifosh P, Zaremba JD, Danielson NB, Losonczy A. SIMA: Python software for analysis of dynamic fluorescence imaging data. *Frontiers in neuroinformatics*. 2014; 8:80. [PubMed: 25295002]

- Author Manuscript
- Author Manuscript
- Author Manuscript
- Author Manuscript
62. Ali AB. Presynaptic Inhibition of GABA_A receptor-mediated unitary IPSPs by cannabinoid receptors at synapses between CCK-positive interneurons in rat hippocampus. *Journal of neurophysiology*. 2007; 98:861–869. [PubMed: 17567776]
63. Cea-del Rio CA, Lawrence JJ, Erdelyi F, Szabo G, McBain CJ. Cholinergic modulation amplifies the intrinsic oscillatory properties of CA1 hippocampal cholecystokinin-positive interneurons. *The Journal of physiology*. 2011; 589:609–627. [PubMed: 21115639]
64. Younts TJ, Chevaleyre V, Castillo PE. CA1 pyramidal cell theta-burst firing triggers endocannabinoid-mediated long-term depression at both somatic and dendritic inhibitory synapses. *The Journal of neuroscience : the official journal of the Society for Neuroscience*. 2013; 33:13743–13757. [PubMed: 23966696]
65. Lee SH, Foldy C, Soltesz I. Distinct endocannabinoid control of GABA release at perisomatic and dendritic synapses in the hippocampus. *The Journal of neuroscience : the official journal of the Society for Neuroscience*. 2010; 30:7993–8000. [PubMed: 20534847]
66. Vida I, Halasy K, Szinyei C, Somogyi P, Buhl EH. Unitary IPSPs evoked by interneurons at the stratum radiatum-stratum lacunosum-moleculare border in the CA1 area of the rat hippocampus in vitro. *The Journal of physiology*. 1998; 506(Pt 3):755–773. [PubMed: 9503336]

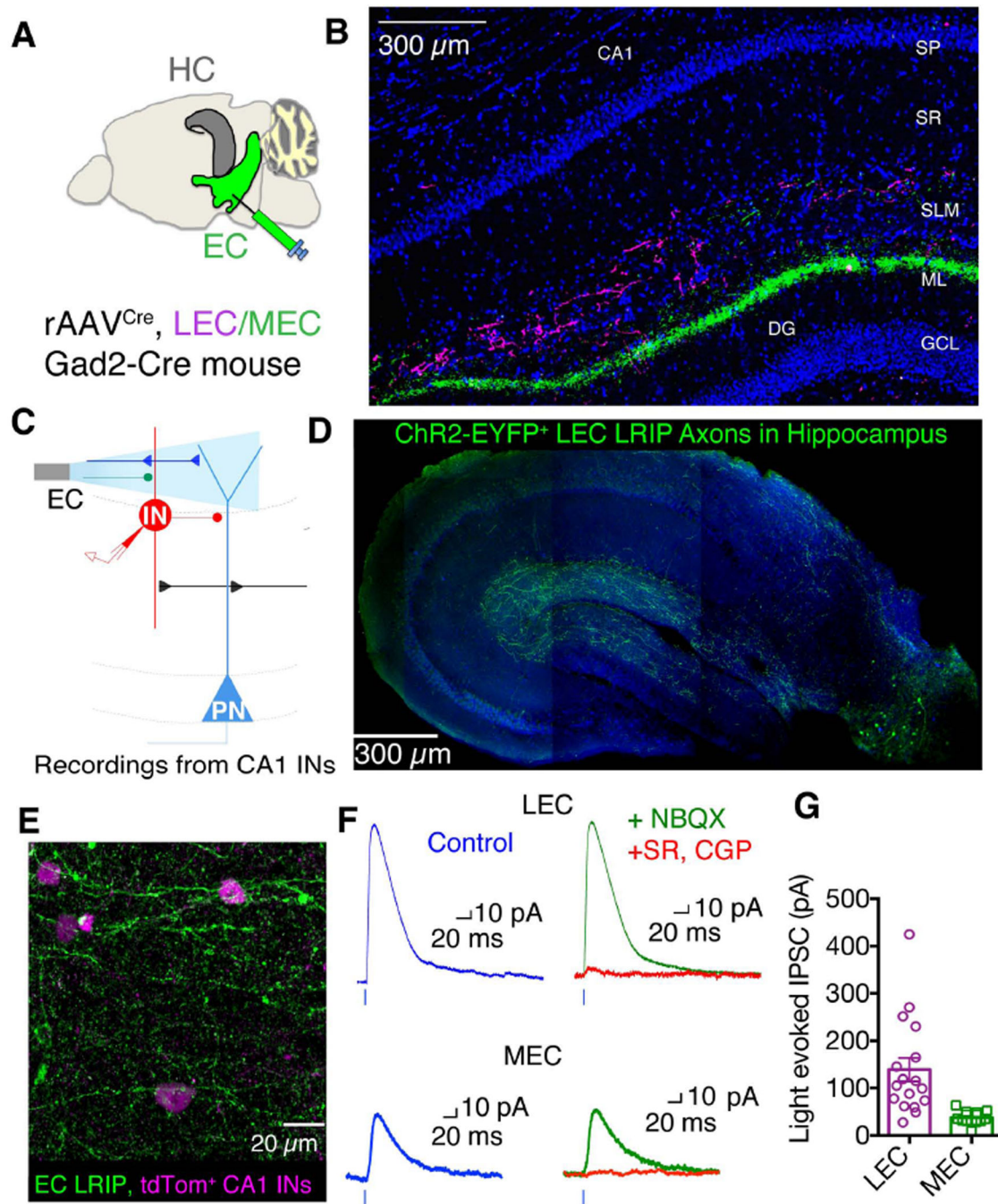


Fig. 1. Lateral entorhinal cortex provides strong long-range GABAergic inputs to local CA1 inhibitory neurons

A. LEC and MEC viral injection sites (in green) and their hippocampal target (HC, in grey).

B. TdTomato-labelled (magenta) and GFP-labelled (green) axons in SLM of CA1 from LEC and MEC *Gad2-Cre*⁺ LRIPs, respectively. DAPI stain in blue. C. Scheme of experiment to functionally map impact of LRIPs from LEC or MEC on CA1 INs at SR/SLM border.

ChR2-EYFP was virally expressed in GABAergic neurons in the LEC or MEC using rAAV^{Cre} injections in *Gad2-Cre* mice. Patch clamp recordings obtained from a CA1 IN (red)

Author Manuscript
Author Manuscript
Author Manuscript
Author Manuscript
Author Manuscript

at the border of SR/SLM that targets the CA1 PN dendrite (light blue). 470 nm laser light focused on SLM photostimulated ChR2⁺ LRIPs (green). **D.** 20× confocal image of ChR2-EYFP⁺ LRIP axons from LEC (green) in hippocampus from *Gad2-Cre* mouse. DAPI staining in blue. **E.** 63× confocal images showing ChR2-EYFP⁺ LRIP axons from LEC (green) in CA1 SLM region impinging upon tdTomato⁺ IN soma (magenta). **F.** Light-evoked inhibitory postsynaptic currents (IPSCs) recorded from CA1 SR/SLM INs in normal extracellular solution (control, blue) and in presence of glutamate receptor blockers (10 μM NBQX and 100 μM D-APV, green trace) or GABA receptor antagonists (2 μM SR95531 and 1 μM CGP55845, red trace), see fig. S1 for statistics. **G.** Bar (Mean ± SEM) and scatter (individual cells) plot of the light-evoked IPSCs (pA, V_m = +10 mV) from responsive CA1 SR/SLM INs with ChR2 expressed in LEC (magenta, 139 ± 24.8 pA, n = 17) or MEC (green, 37.7 ± 4.5 pA, n = 11; P < 0.005, t-test, LEC LRIP versus MEC LRIP).

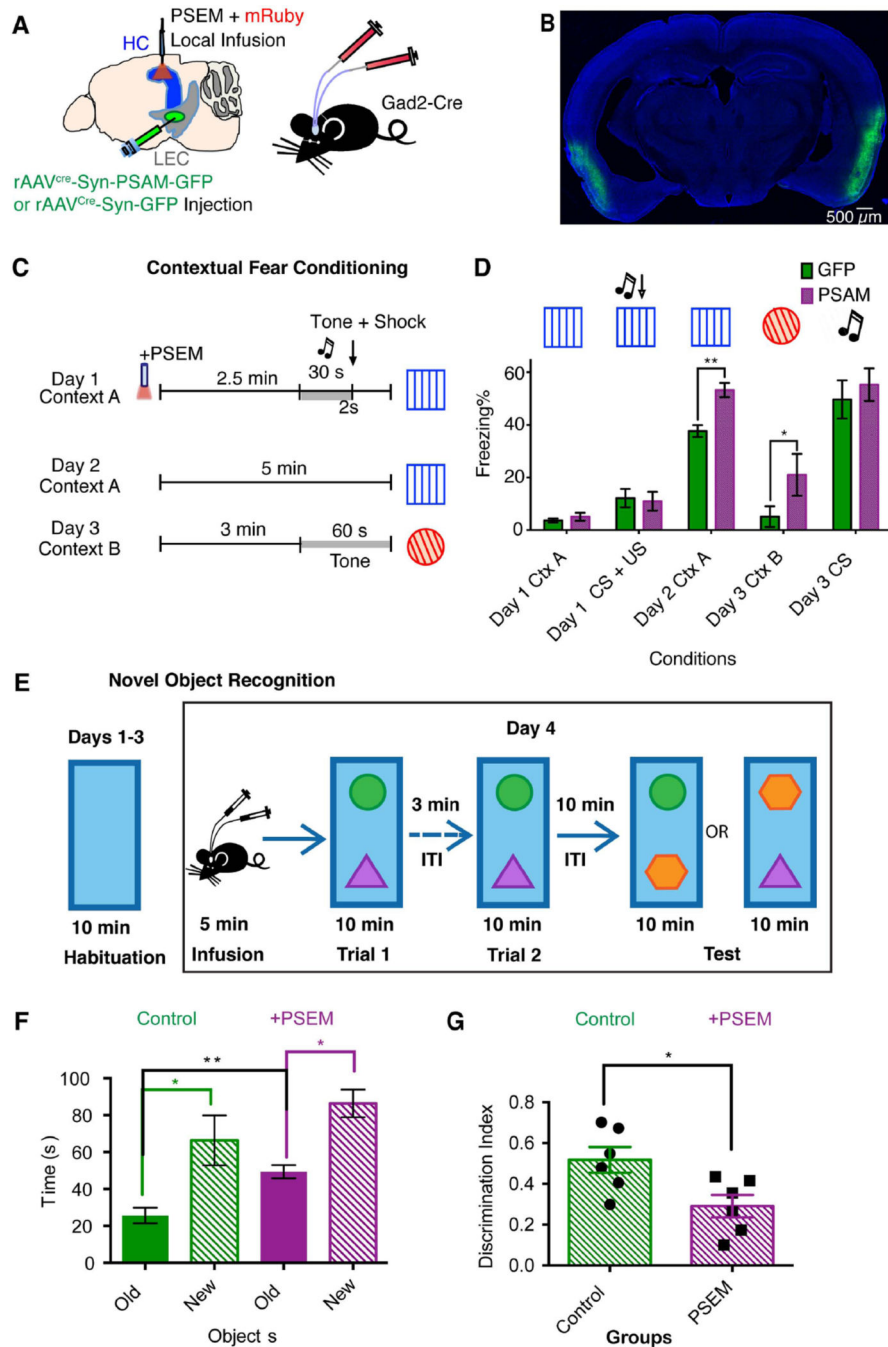


Fig. 2. Silencing LEC LRIPs in CA1 alters both context and object recognition memory

A. Diagram of the experimental design. Gad2-Cre mice were injected with AAV^{Cre} to express GFP or PSAM in LEC. PSEM was delivered bilaterally to the CA1 region just prior to the training phase of memory tasks. B. Confocal image ($5\times$) of coronal section from a Gad2-Cre mouse injected in LEC with an AAV^{Cre} expressing PSAM-2A-GFP, showing expression of GFP (green) in LEC (DAPI in blue). C. Scheme of contextual fear conditioning (see Methods). On day 1, mice were exposed to Context A, then given a tone followed by footshock. On day 2, mice were re-exposed to Context A. On day 3, mice were

exposed to novel Context B, followed by a tone. PSEM was delivered just prior to training in mice expressing GFP (control) or PSAM in LRIPs. **C.** Bar plot (mean \pm SEM) of time spent freezing (GFP, green; PSAM, purple): Day 1, in Context A before (Ctx A) and after (CS +US) footshock; Day 2, during recall testing in Context A; Day 3, in novel Context B before (Ctx B) and after cued tone (Day 3 CS.). Two-way repeated-measures ANOVA revealed no significant difference between groups in freezing on day 1 in Context A (treatment \times time F (6, 105) = 0.8055, P = 0.5679; **treatment F (1, 105) = 3.655, P = 0.0586**; time F (6, 105) = 8.583, P < 0.0001). There was a significant difference in freezing between groups in Context A on day 2 (treatment \times time F (4, 48) = 0.8918, P = 0.4761; **treatment F (12, 48) = 5.069, P < 0.0001**; time F (4, 48) = 11.75, P < 0.0001) and in Context B (no tone) on day 3 (treatment \times time F (3, 45) = 1.230, P = 0.3069; **treatment F (15, 45) = 2.246, P < 0.0186**; time F (3, 45) = 53.01, P < 0.0001). The PSAM group showed significantly greater freezing on Day 3 in context B versus context A on Day 1 prior to footshock (treatment F (12, 24) = 5.332; time F (2, 24)=19.76; P < 0.0002). The GFP control group showed no significant difference in freezing in context A on Day 1 versus context B on Day 3 (treatment F (18, 18) = 0.4932; time F(2, 18) = 12.84; P = 0.928 n.s.). **E.** Schematic of experiment to test effect of silencing LEC LRIPs on novel object recognition (NOR). Mice were exposed to two objects in training trials 1 and 2, followed by a test trial in which one (now familiar or “old”) object was replaced by a novel (“new”) object. Prior to training, mice were infused with 0.5 μ l of either 15 μ M PSEM³⁰⁸ plus the dye miniRuby (silenced group, + PSEM) or miniRuby alone (control). Both groups expressed PSAM in LEC. **F.** Bar plots of time spent with familiar (old) versus novel (new) object in test trial. The PSEM treated group explored the old object for 49.38 ± 3.55 s (P < 0.005 versus control) and the new object for 86.38 ± 7.49 s (n = 6; P < 0.05, new versus old object, paired t-test). **G.** The discrimination index, calculated as (time spent exploring the new object – time spent exploring old object)/(total exploration time), was significantly greater in control versus PSEM-treated mice (P < 0.05, paired t-test).

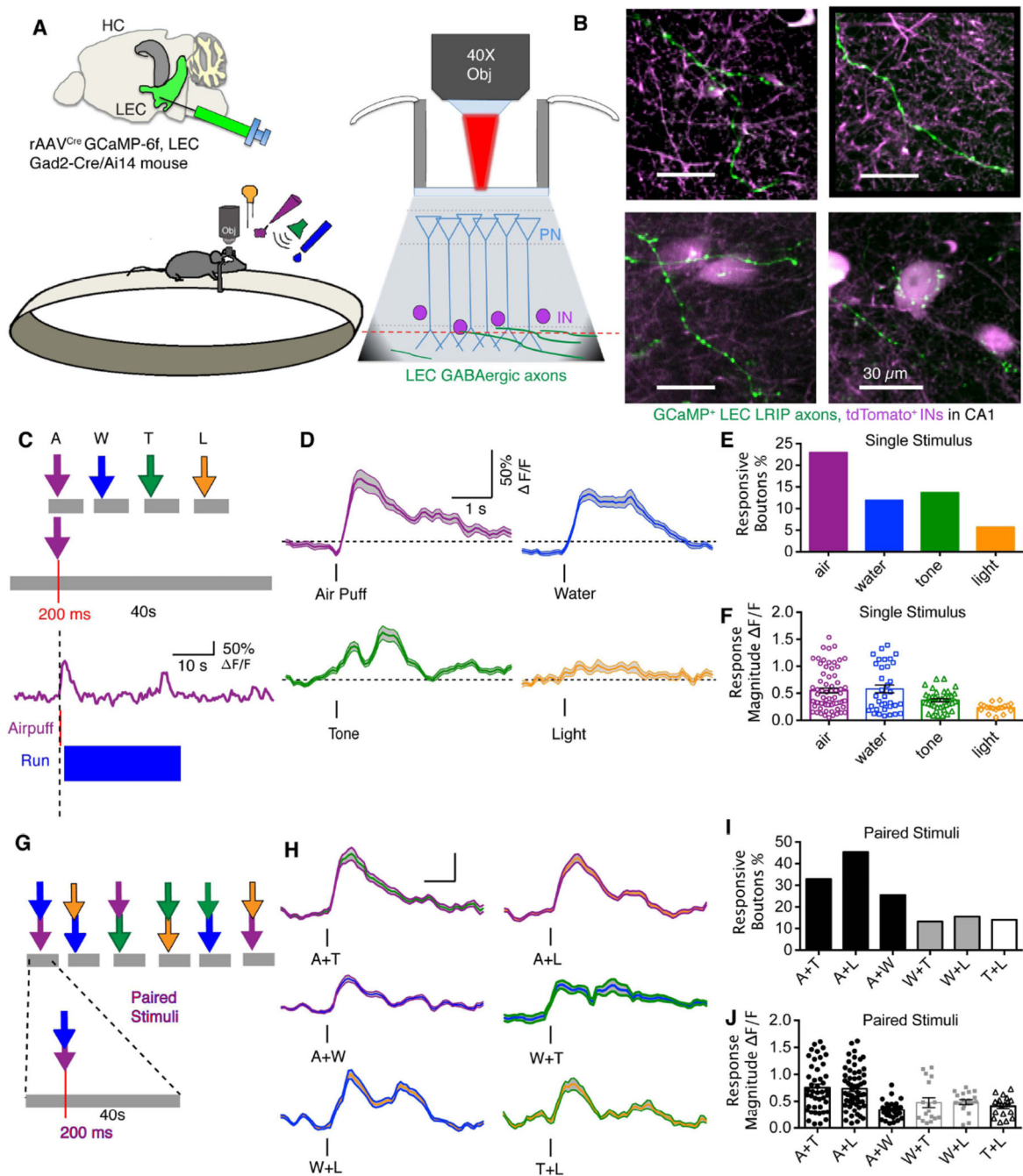


Fig. 3. Functional imaging of sensory coding in LEC LRIPs in SLM of CA1

A. Diagram of *in vivo* imaging experiment. GCaMP6f was expressed in dorsal LEC, by injecting cre-dependent rAAV in Gad2-Cre/Ai 14 mice that also expressed tdTomato in all GABAergic neurons. A 40 \times water immersion objective was used for two-photon imaging through a cranial window over CA1 in head-fixed awake mice during multimodal sensory and behavioral stimuli presentation. **B.** Four examples of time averaged images of GCaMP6f fluorescence in LEC LRIP axons in SLM (green) with tdTomato labeling CA1 interneurons (magenta). **C.** Experimental design of single stimulus protocol. Imaging was performed in

blocks of 4 trials, each 40 s in duration. After a 10 ± 3 s baseline one of four types of stimuli—aversive airpuff (A), water drop (W), tone (T) and light (L)—were presented in random order for 200 ms, except the water drop was limited to 50 ms to prevent satiation. Each block was repeated to obtain at least 5 trials per stimulus. The animal's behavioral response (running and licking) was monitored. F/F traces showing increased Ca^{2+} signal in a single bouton on an LRIP axon in response to airpuff. **D.** Mean (\pm SEM) F/F Ca^{2+} signal (PSTH) from responsive regions-of-interest (ROI) to indicated stimuli. **E.** Percentage of responsive boutons to the stimuli (air = 22.92%, water = 11.96%, tone = 13.64% and light = 5.65%). **F.** Scatter and mean (\pm SEM) plots of F/F signals from individual responsive boutons (air = 0.55 ± 0.05 , n = 68; water = 0.58 ± 0.07 , n = 35; tone = 0.37 ± 0.03 , n = 37; light = 0.23 ± 0.02 , n = 18) **G.** Experimental protocol: Imaging was performed as described above, but in response to pairs of stimuli, presented in blocks of 10 trials, each 40 s long. Stimuli were randomized and paired stimuli were interleaved with single stimulus presentations. **H.** Mean (\pm SEM) F/F Ca^{2+} signal (PSTH) from responsive ROIs to paired stimuli. **I.** Percentage of responsive boutons for paired stimuli (A+T = 32.8%; A+L = 45.3%; A+W = 25.4%; W+T = 13.3%; W+L = 15.6%; T+L = 14.1%). **J.** Scatter and mean (\pm SEM) plots of F/F signals to paired stimuli from individual responsive boutons (A+T = 0.76 ± 0.07 , n = 44; A+L = 0.74 ± 0.05 , n = 58; A+W = 0.34 ± 0.03 , n = 31; W+T = 0.48 ± 0.09 , n = 17; W+L = 0.49 ± 0.04 ; T+L = 0.41 ± 0.045 , n = 18).

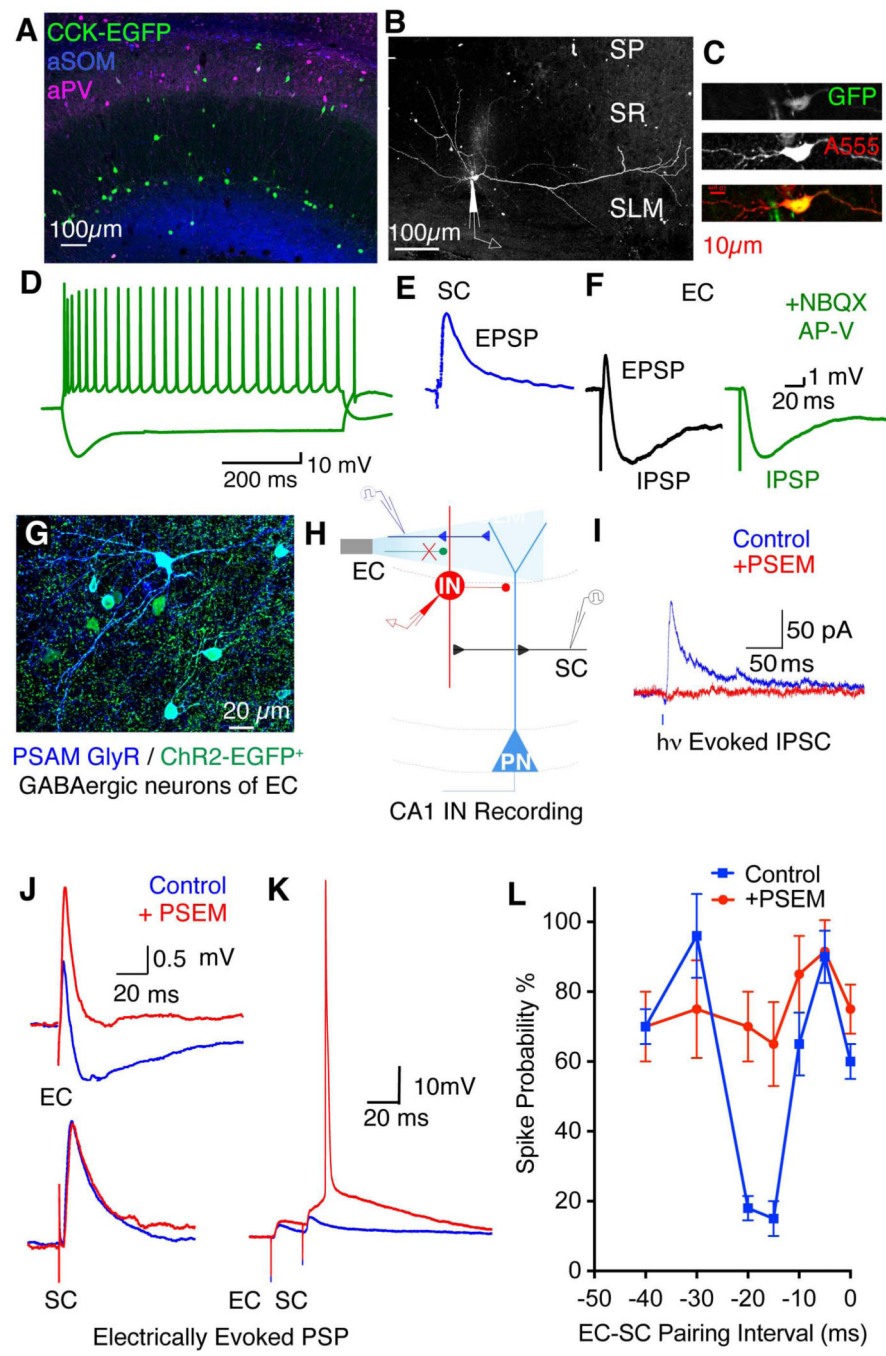


Fig. 4. CCK IN excitation and spike firing is suppressed 15–20 ms after LRIP activation

A. Confocal projection image (left) showing CCK⁺ (GFP, green), PV⁺ (immunostained, magenta) and SOM⁺ (immunostained, blue) IN soma in a hippocampal section from a CCK-Cre/DLX-Flpe/RCE dual reporter mouse. Note abundant GFP⁺ CCK IN soma at the SR/SLM border. **B.** Z-axis projection image (right) of a GFP⁺ CCK IN at SR/SLM border filled with neurobiotin-Alexa 555 (white). **C.** Zoomed in image of IN in **B**, showing GFP (top) and Alexa 555-neurobiotin (middle) colabeling (bottom, yellow). Scale bar, 10 μ m. **D**–**F**. Whole cell voltage recordings from IN in **B**, **C**. **D**. Spike firing and voltage sag in **E**. **F**. EPSP and IPSP. **G**. Confocal image of PSAM GlyR⁺ / ChR2-EGFP⁺ GABAergic neurons of EC. **H**. Schematic of CA1 IN Recording. **I**. hv Evoked IPSC. **J**. Electrically Evoked PSP. **K**. Electrically Evoked PSP. **L**. Spike Probability % vs EC-SC Pairing Interval (ms).

response to 700 ms, 200 pA depolarizing and hyperpolarizing current steps, respectively. **E.** Depolarizing PSP evoked by SC stimulation. **F.** Mixed depolarizing and hyperpolarizing PSP evoked by EC stimulation (black). Bath application of NBQX (10 μ M) and D-APV (100 μ M) blocked the depolarization but not the hyperpolarization (green trace). **G.** 63 \times projection image of PSAM (α -BTX-Alexa 647, blue) and ChR2-EGFP (green) showing co-expression in ~75% of EC INs in brain section from a Gad2-Cre mouse injected in LEC and MEC with rAAV^{Cre}. **H.** Experimental scheme showing whole cell recording from a CA1 SR/SLM IN with photostimulation of LRIPs or electrical activation of EC inputs. **I.** Voltage-clamped IPSCs from CCK+ IN (verified by posthoc staining) evoked by photostimulation of LRIPs in absence (blue trace) or presence (red trace) of PSEM (3 μ M). **J.** Voltage responses in CA1 IN evoked by electrical stimulation of EC (top) or SC (bottom) inputs in absence (control, blue trace) and presence (red trace) of PSEM. **K.** Voltage responses of CA1 SR/SLM IN to paired electrical stimulation of EC and SC inputs (20 ms delay) in the absence (blue trace) and presence (red trace) of PSEM. **L.** Mean probability of SR/SLM IN spike firing (percent of stimuli eliciting a spike \pm SEM) in response to paired EC-SC stimulation as a function of pairing interval in absence and presence of PSEM (spike probability with -20ms EC-SC pairing: control = 18 \pm 4%; PSEM = 70 \pm 10%; $P < 0.005$, $n = 7$).

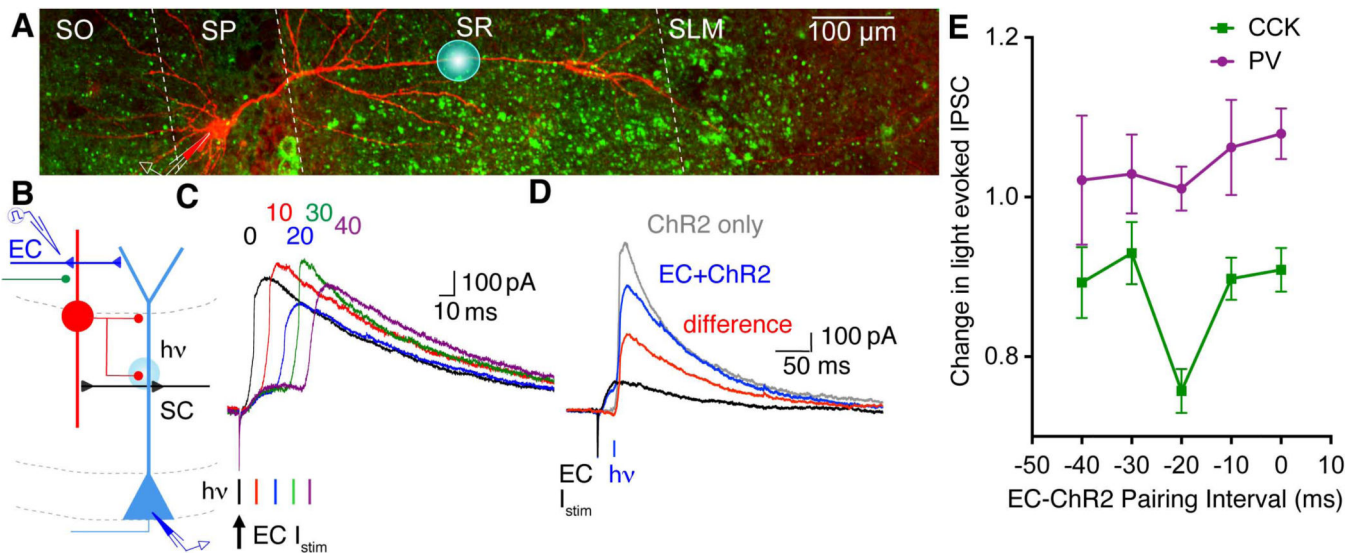


Fig. 5. LRIPs suppress SC-evoked FFI from CCK+ SR/SLM INs

A. Confocal projection image of a CA1 PN filled with Alexa 594 (red) in a slice where CCK+ INs expressed ChR2-EGFP (green). Blue circle represents the perimeter of 470 nm light stimulus. **B.** Experimental scheme depicting somatic recording from a CA1 PN (red); electrical stimulation of EC inputs in SLM was paired at variable delays with photostimulation of CCK+ INs. **C.** IPSCs evoked by photostimulation of CCK INs (*hv*) recorded from soma of a voltage-clamped CA1 PN (+10 mV) during paired electrical stimulation of EC inputs (arrow) at 0, 10, 20, 30 and 40 ms delays. **D.** IPSCs in CA1 PNs evoked by electrical stimulation of EC inputs and photostimulation of CCK+ INs. Grey trace (ChR2 only), CA1 PN IPSC evoked by photostimulation of CCK+ IN. Black trace (EC), CA1 PN IPSC evoked by electrical stimulation of EC input. Blue trace (EC+ChR2), net IPSC evoked by pairing EC electrical stimulation with photostimulation of CCK+ IN (20 ms delay). Red trace (difference), Inferred CCK+ IN IPSC evoked when EC electrical stimulation preceded photostimulation of CCK+ IN by 20 ms. Trace obtained by subtracting EC-evoked IPSC (black trace) from IPSC evoked during paired stimulation (blue trace). **E.** Effect of pairing interval on EC-dependent suppression of IPSC evoked by photostimulation of CCK+ INs or PV+ INs. Mean (\pm SEM) amplitude of photostimulation-evoked IPSC during pairing with EC stimulation (measured as in **D**) normalized by photostimulated IPSC amplitude in absence of EC stimulation, plotted versus pairing interval. ChR2-EGFP expressed in either PV+ INs (magenta, 1.01 ± 0.03 fold change at -20 ms pairing interval, $P = 0.3319$, paired two-tailed t-test, $n = 5$) or CCK+ INs (green, 0.76 ± 0.03 fold decrease in IPSC at -20 ms pairing interval, $P = 0.0006$, paired two-tailed t-test, $n = 9$).

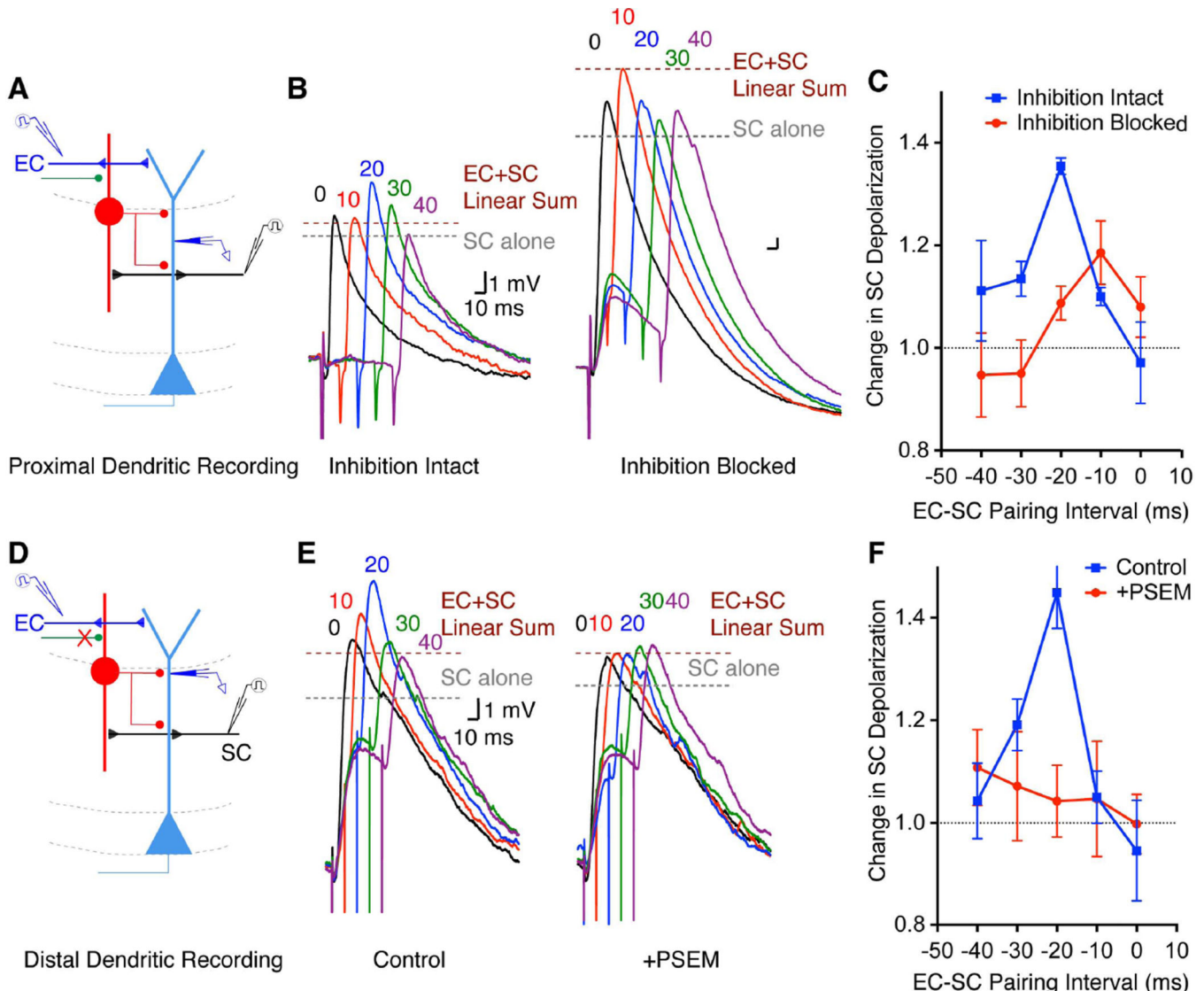


Fig. 6. LRIPs enhance CA1 pyramidal neuron dendritic depolarization in response to SC stimulation through disinhibition

A. Experimental scheme for assessing the synaptic response in CA1 PN dendrites to paired EC-SC electrical stimulation. Panel shows approximate locations of EC and SC stimulation electrodes and dendritic recording pipette. **B.** Dendritic voltage responses to paired EC-SC electrical stimulation at indicated delays (SC after EC), in absence (left) or presence (right) of SR95531 (2 μ M) and CGP55845 (1 μ M). Grey dashed line, amplitude of PSP evoked by SC stimulation alone. Red dashed line, predicted linear sum of PSPs evoked by EC and SC stimulation alone. **C.** Summary plot (mean \pm SEM) of paired EC-SC peak PSP normalized by PSP evoked by SC stimulation alone recorded in CA1 PN proximal dendrites in absence (blue squares) and presence (red circles) of GABAR blockers (EC-SC –20 ms pairing: with inhibition intact, fold change = 1.35 ± 0.02 ; with inhibition blocked, fold change = 1.08 ± 0.03 ; P = 0.001, Two way ANOVA with Sidak multiple comparisons test, n = 5). **D.** Experimental scheme to determine how silencing LRIPs (denoted by X) affects PSP in CA1 PN distal dendrites during paired EC-SC stimulation. PSAM expressed in LEC GABAergic

Author Manuscript
Author Manuscript
Author Manuscript
Author Manuscript
Author Manuscript

neurons in GAD2-Cre mouse with AAV^{Cre}. **E.** CA1 PN distal dendrite PSPs evoked by paired stimulation of EC-SC inputs at indicated intervals, first in absence (left) and then in presence (right) of PSEM. **F.** Mean (\pm SEM) PSP amplitude recorded in CA1 PN distal dendrites evoked by paired EC-SC stimulation normalized by PSP evoked by SC stimulation alone, in absence (blue squares) and presence (red dots) of PSEM. PSEM significantly reduced the effect of paired EC-SC stimulation at -20 ms delay to increase PSP size (Control, 1.45 ± 0.07 fold increase; PSEM, 1.04 ± 0.07 fold increase; $P < 0.001$, Two way ANOVA with Sidak multiple comparisons test, $n = 8$).

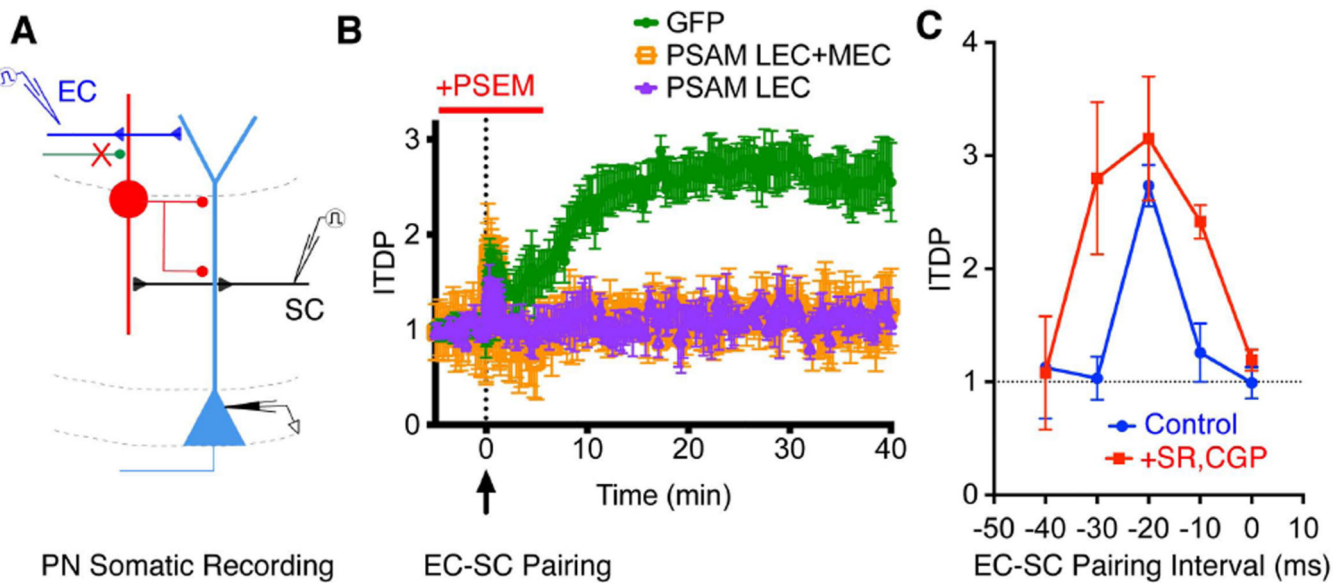


Fig. 7. LEC LRIPs enable induction of ITDP in CA1 PNs

A. Experimental scheme to assess role of LRIPs in ITDP. PSAM or GFP was expressed in GABAergic neurons in LEC alone or in both LEC and MEC. ITDP was induced by pairing EC-SC stimulation at 1 Hz for 90 s with a -20 ms delay. **B.** Pairing protocol induces a 2.65 ± 0.23 fold increase in the SC-evoked depolarization in the CA1 PN soma (ITDP relative to baseline PSP) when PSEM is applied to slices expressing GFP in LEC GABAergic neurons (green, $n = 5$, $P < 0.0001$ two tailed t-test, before versus after ITDP pairing). ITDP is absent when the pairing protocol is applied with PSEM present in slices expressing PSAM in GABAergic neurons in LEC alone (purple triangles, 1.09 ± 0.12 fold potentiation, $n = 4$, $P = 0.114$, two tailed t-test before versus after ITDP pairing; $P < 0.0001$, two tailed t-test for ITDP with GFP versus PSAM in LEC). ITDP is also absent in presence of PSEM when PSAM was expressed in both LEC and MEC (orange squares, 1.10 ± 0.31 fold potentiation, $n = 4$, $P = 0.189$, two tailed t-test pre vs. post ITDP pairing; $P < 0.0001$, two tailed t-test for ITDP with GFP versus PSAM in LEC+MEC). Peak PSP value normalized to value 5 mins prior to ITDP induction. Mean fold potentiation obtained by averaging normalized PSP values during the 25–30 min period after ITDP induction. **C.** ITDP tuning curve showing potentiation (mean \pm SEM) as a function of EC-SC pairing interval. Blue circles, with inhibition intact (-10 ms interval, 1.25 ± 0.26 fold change, $n = 4$; -20 ms interval, 2.74 ± 0.18 fold change, $n = 5$; -30 ms interval, 1.03 ± 0.19 fold change, $n = 4$). Red squares, ITDP with GABAR antagonists applied only during induction protocol (-10 ms, 2.41 ± 0.15 fold change, $n = 5$; -20 ms, 3.15 ± 0.55 fold change, $n = 7$; -30 ms, 2.8 ± 0.67 fold change, $n = 4$). Inhibition blocked versus intact, no significant difference, $P = 0.105$ two way ANOVA.

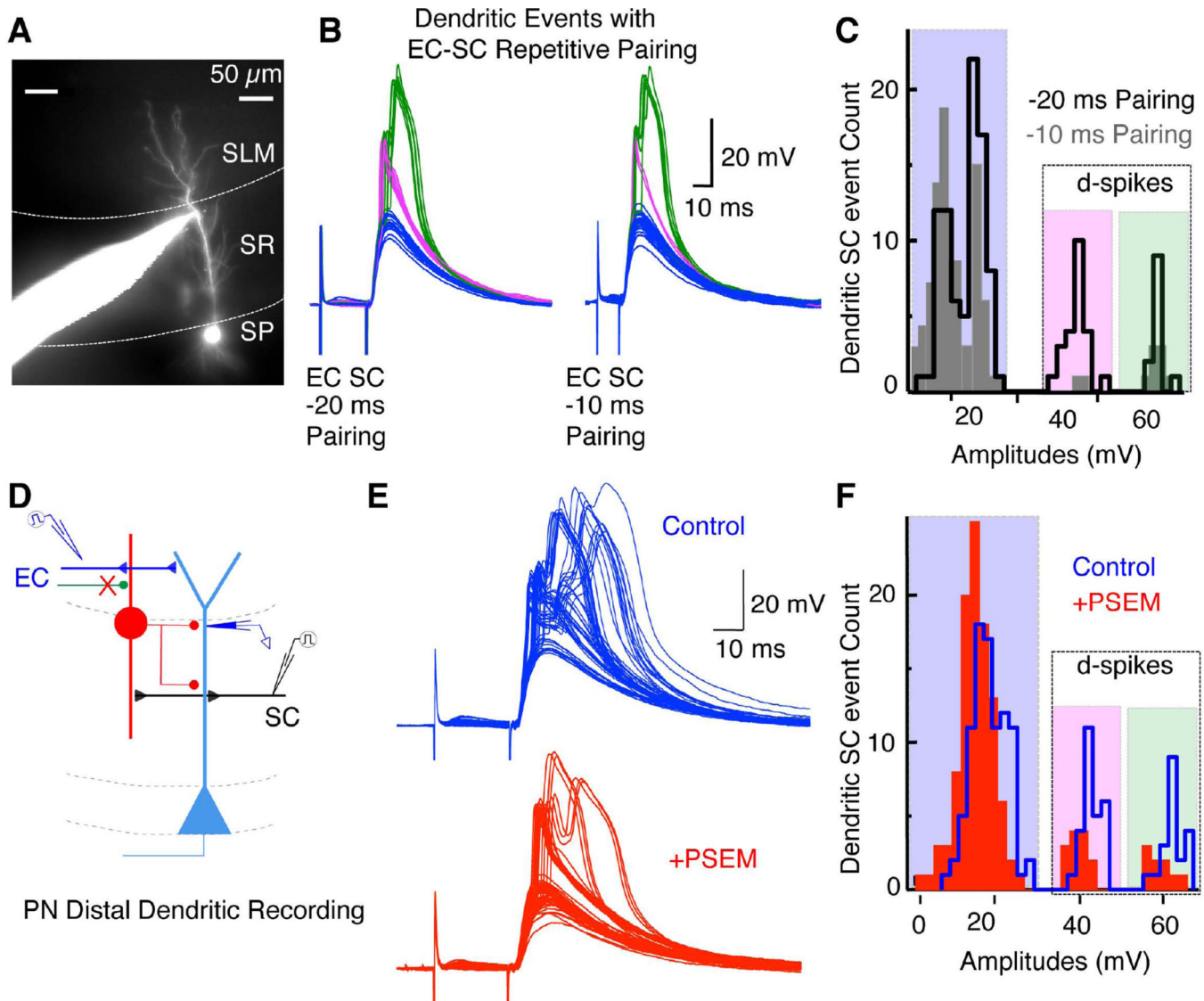
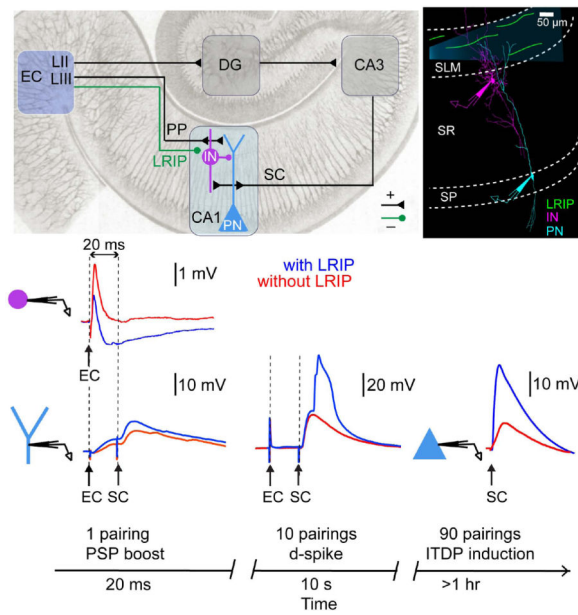


Fig. 8. EC-SC pairing at -20 ms interval induces dendritic spikes

A. Image showing CA1 PN filled with Alexa 594 during a distal dendritic recording. **B.** Dendritic PSPs (blue), brief spikes (magenta) and long spikes (green) evoked by 10—30s repetitive pairing of EC-SC inputs at 1 Hz with -20 or -10 ms pairing intervals. During first 5–10 paired stimuli only subthreshold PSPs were observed. **C.** Histograms of the peak dendritic voltage response evoked by a train of 30 paired EC-SC stimuli at 1 Hz, using a -20 ms (black open bars) or -10 ms (gray filled bars) pairing interval ($P < 0.005$, t-test within cell comparisons for -20 ms vs -10 ms; $n = 3$). Responses were classified based on amplitude and duration as subthreshold PSPs (blue) or dendritic spikes (magenta, brief spikes; green, long spikes). **D.** Experimental scheme to assess role of LRIPs in dendritic spikes firing. PSAM was virally expressed in LEC of Gad2-Cre mice. **E. and F.** Distal dendritic responses (**E**) and event amplitude histograms (**F**) to paired EC-SC stimulation at 1 Hz using a -20 ms delay interval in absence (blue) and then presence (red) of PSEM ($P < 0.0001$, t-test within cell comparisons, Control vs. +PSEM; $n = 3$).



Long-range inhibitory projections gate cortico-hippocampal information flow

Top Left, Entorhinal cortex (EC) excites CA1 pyramidal neurons (PN) directly (PP) and indirectly (ECe → DGe → CA3e → CA1). EC also sends direct long-range inhibitory projections (LRIP) to CA1. *Top Right*, LRIPs (green) and dye-filled CA1 PN and inhibitory interneuron (IN). *Bottom*, Disinhibitory effect of LRIPs. IN (top) and PN (bottom) recordings with LRIPs active (blue) or silenced (red). EC stimulation evokes mixed excitation/inhibition (EPSP/IPSP) in IN. Schaffer collateral, SC-evoked dendritic depolarization is enhanced when preceded by EC stimulation (20 ms delay) because LRIPs inhibit INs (disinhibition). Ten or more EC-SC paired stimuli (1 pair/s) trigger PN dendritic spikes (d-spikes). 90 s of EC-SC pairing induces input timing-dependent plasticity (ITDP) leading to long-term potentiation in SC-evoked PN excitation. LRIP silencing (red traces) decreases dendritic depolarization and spike firing, and blocks ITDP.